

On-chip phase-change photonic memory and computing

Zengguang Cheng^a, Calos Ríos^a, Nathan Youngblood^a, Wolfram HP Pernice^b, Harish Bhaskaran^{*a}

^aDepartment of Materials, University of Oxford, 16 Parks Road, Oxford OX1 3PH, UK

^bInstitute of Physics, University of Muenster, Heisenbergstr, 11, 48149 Muenster, Germany

ABSTRACT

The use of photonics in computing is a hot topic of interest, driven by the need for ever-increasing speed along with reduced power consumption. In the existing computing architectures, photonic data storage would dramatically improve the performance by reducing the latencies associated with electrical memories. At the same time, the rise of ‘big data’ and ‘deep learning’ is driving the quest for non-von Neumann and brain-inspired computing paradigms. To succeed in both aspects, we demonstrate a non-volatile multi-level photonic memory avoiding the von Neumann bottleneck in the existing computing paradigm and a photonic synapse resembling the biological synapses for brain-inspired computing using phase-change materials ($\text{Ge}_2\text{Sb}_2\text{Te}_5$).

Keywords: On-chip photonics, Phase-change materials, memory, brain-inspired computing, synapse

1. INTRODUCTION

The performance of our modern computers based on von Neumann architecture is limited by the traffic jam of the data and instructions shuttling between processors and memories which is called the von Neumann bottleneck¹. At the same time, the emerging of big data², internet of things (IOT)³ and artificial intelligence⁴ is driving the necessary requirements for novel technologies and materials to overcome the von Neumann bottleneck and build an ultra-fast and energy-efficient computing system. The use of photonics in computing is a hot topic of interest, due to its super-fast speed and greatly reduced power consumption⁵.

To succeed in next generation computing paradigm, photonic computing needs new concepts – either nonlinear photonic devices to replace electrical components to speed up the von Neumann bottleneck or a completely different approach based on brain-inspired computing.

With the existing von Neumann architecture, data transfer and storage are highly desirable by optical means attribute to high speed, large bandwidth and low crosstalk of optical communication^{5,6}. However, on-chip implementation of photonic memories using electronic circuits is a big challenge⁷. A full-optical non-volatile photonic memory is preferable to be developed⁸. On the other hand, inspired by the amazing capabilities of the brain in performing learning, emotion and intelligent cognition⁹, it is attractive to mimic the structures and functions of the brain using solid state devices, which leads to a new form of computing architecture, known as neuromorphic computing¹⁰. It's promising to combine photonics with neuromorphic computing to obtain unique capabilities and functionalities.

To implement the memory and computing applications, we need novel nonlinear materials. Due to the high contrast between the crystalline and amorphous states of their electrical and optical properties¹¹, phase-change materials (PCMs) have been commercially used in optical data storage (CD, DVD, Blu-ray, etc.)¹² and been intensively studied as electronic memories¹³⁻¹⁵. Particularly, chalcogenide-based PCMs can be switched between crystalline and amorphous states with response to heat, electrical and optical stimuli¹⁶ (**Fig.1a**). As a demonstration, we use the well-studied PCMs, $\text{Ge}_2\text{Sb}_2\text{Te}_5$ (GST) because of its good performance in data retention^{11,16}, state contrast¹⁷ and energy efficiency⁸.

Herein, we discuss the two concepts based on our recent research on integrated photonic memory and computing using chalcogenide phase-change materials, specifically GST.

*harish.bhaskaran@materials.ox.ac.uk; phone 44 18652 73772; <http://nanoeng.materials.ox.ac.uk>

2. MATERIALS, METHODS AND CONCEPTS

2.1 Fabrication and measurement

The photonic devices were fabricated on a $\text{Si}_3\text{N}_4/\text{SiO}_2$ wafer as reported previously^{8,17}. Electron beam lithography (JBX-5500ZX, 50 kV, JEOL) was used to define the waveguide structure on the wafer with negative tone resist (Ma-N 2403) spin coated, followed by reactive ion etching (PlasmaPro 80, Oxford Instruments) in $\text{CHF}_3/\text{O}_2/\text{Ar}$ to etch down 165 nm or 300 nm of Si_3N_4 . Another layer of electron beam lithography on positive resist (PMMA, Micro Chem.) was used to define the pattern for PCMs units and 10 nm GST/10 nm ITO was subsequently sputter deposited. After sputtering and lift-off process, the devices were thermal annealed at $\sim 250^\circ\text{C}$ for 5-10 mins to completely crystallize the GST layers, ready for optical measurements.

The real-time measurements on the optical transmission of the photonic devices with optical pulse switching was performed by a probe-pump technique described previously⁸. Briefly, a low-power probe laser and a high-power pump laser working at different wavelengths were guided through photonic devices from opposite directions. Optical circulators were applied to guide one laser into the device while extracting the other laser out to detectors. To suppress interference between the two lasers, we used optical band pass filters (OTF-320, Santec) in the probe/pump routes.

A CW diode laser (TSL-550, Santec) as a probe laser was used to investigate the transmission of the photonic devices. The pump pulse was achieved using a CW diode laser (N7711A, Keysight) modulated by an electrical pulse generator (AFG 3102C, Tektronix). Subsequently, the optical pulse was amplified by a low-noise fiber amplifier (AEDFA-CL-23, Amonics).

2.2 Concepts of photonic memory and computing

As shown in the left panel **Fig. 1b**, a single GST unit (width $w_{\text{GST}} = 0.5\sim 4\ \mu\text{m}$) is fabricated on top of a Si_3N_4 waveguide (width $w_{\text{wg}} = 1.3\ \mu\text{m}$) with 165 nm etched down. Due to the high contrast of refractive index and absorption between crystalline and amorphous GST film, the optical transmission through the waveguide is highly dependent on the states of GST. By using different power of optical pulse to switch GST film to some specific intermediate state, we can achieve multiple levels stored in the photonic memory corresponding to different optical transmissions and GST states (**Fig. 1b**, right panel).

On the other hand, we developed a photonic synapse inspired by mammalian brain-like computing, shown in **Fig. 1c**. Different from the structure of photonic memory in **Fig. 1b**, the photonic synapse is based on a full etched (300 nm) tapered waveguide ($w_{\text{wg}} = 1.3\ \mu\text{m}$ and $w_c = 0.8\ \mu\text{m}$) with multiple GST units on top. The transmission of this photonic synapse has a strong and monotonic dependence on the number of optical pulses which makes each transmission level (weight) could be accessed with a specific number of optical pulses, an ideal candidate for photonic neuromorphic computing. In mammalian brain, each neuron is connected by thousands of other neurons with the connections called synapses (**Fig. 1c**, right panel). The connection strength is synaptic weight which has the plasticity to be modulated by the time delay between pre- and post-neurons. This plasticity is believed to be the reason of learning and memory. We will demonstrate the photonic synapse does have the plasticity.

3. DATA AND RESULTS

3.1 Phase-change photonic memory

The photonic device for memory application is fabricated as the design in **Fig. 1b**. As described in the above section, the GST layer ($w_{\text{GST}} = 2\ \mu\text{m}$) have been fully crystallized as the initial state (level ‘0’) for optical measurements. After stabilized for ~ 10 mins, a single optical pulse (10 ns width) was applied through the pump route and the optical transmission (T) as the memory level was monitored at the same time in the probe route.

A pulse with small power (pump power current $I = 526\ \text{mA}$ for the optical amplifier) just above the threshold of switching, was applied to the photonic device which increased the memory level to ‘1’ sustained after the switching. Kept increasing the power of the single pulse, we obtained step-by-step non-volatile memory levels due to gradually amorphization of the GST layer (black arrow in **Fig. 2a**). After the final optical pulse ($I = 550\ \text{mA}$), we reached the level ‘21’ with over 60% change of the optical transmission from the baseline. Afterwards, the photonic device was deliberately re-crystallized to the baseline by single optical pulse (10 ns width) with decreased powers (red arrow in **Fig. 2a**). We achieved 22 levels in total during the amorphization and crystallization processes.

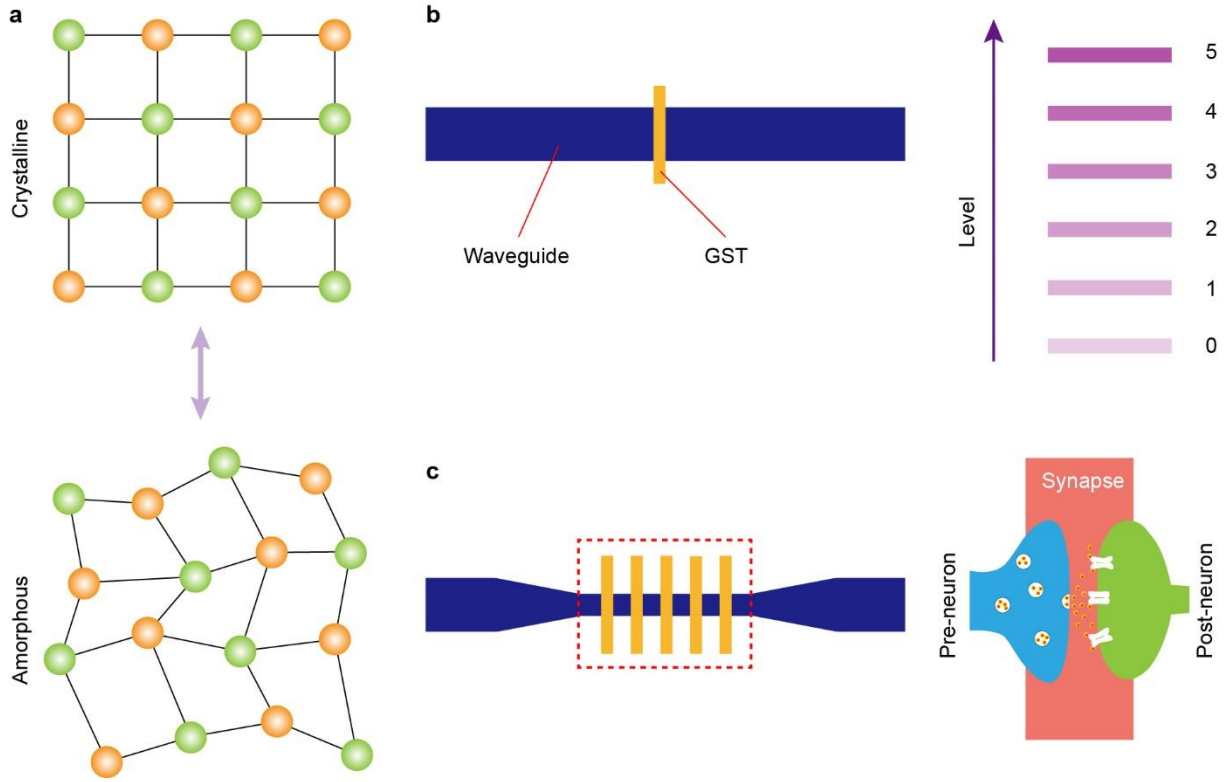


Figure 1. (a) Phase transition between crystalline and amorphous of phase-change materials. (b) Schematic of a GST unit residing on a straight waveguide (left) and its related application in photonic memory (right). (c) Schematic of multiple GST units on a tapered waveguide (left) and its related application in brain-inspired computing.

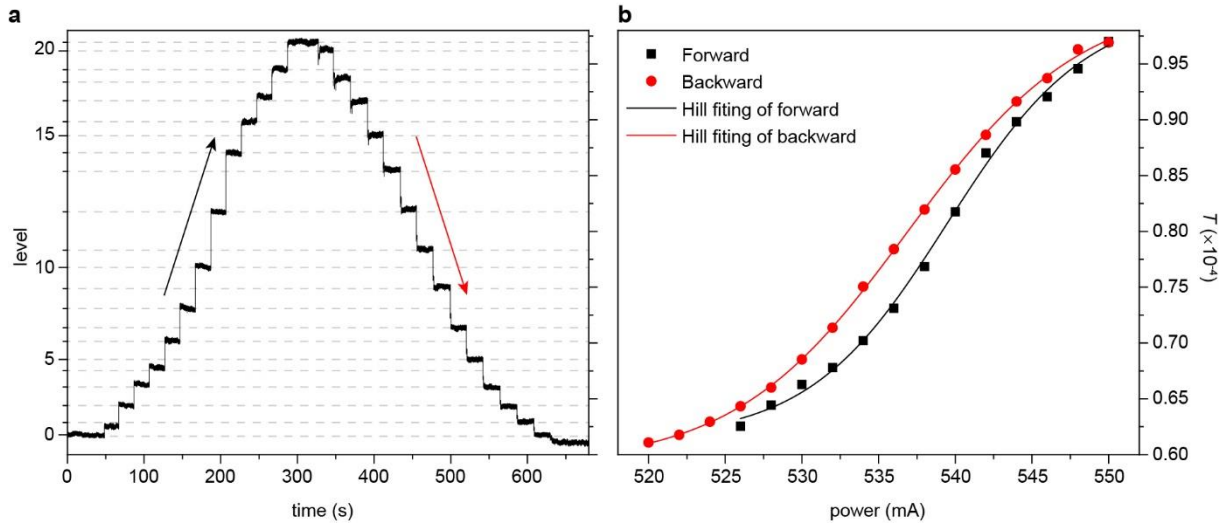


Figure 2. (a) Non-volatile multi-level switching of a typical photonic phase-change memory using a single optical pulse. (b) Optical transmission (memory level) dependence on the switching power of the optical pulses. Black square and red circles corresponds to forward (black arrow) and backward (red arrow) switching directions respectively, as shown in (a). Black and red curves are the fittings to the data using Hill function.

To investigate the switching power dependence on the memory level, we plot the optical transmission (T) as a function of the pump power current (I , linear dependent on the pump power) for both forward and backward switching, shown in Fig. 2b. The data from both switching directions have 'S' shape function dependence on the pump power current, which have threshold, linear and saturation regimes and can be well fitted by Hill function:

$$T = T_1 + \frac{T_0 - T_1}{1 + (I/I_0)^p} \quad (1)$$

Where T_0 and T_1 are the optical transmissions at initial and final states of the photonic device, while I_0 is the pump power current at the middle value of the transmission and p is the Hill coefficient. The detailed fitting parameters of Hill curves in **Fig. 2b** are illustrated in **Table 1**. Notably, to reach a specific level, the power used for amorphization (forward) is always larger than that for re-crystallization (backward), especially in the linear regime (**Fig. 2b**).

3.2 Phase-change photonic synapse

Based on the design in **Fig. 1c**, we fabricated the photonic device as a photonic synapse. Seven GST units (0.75 μm each) were distributed uniformly in the tapered region (10 μm long) of the waveguide and fully crystallized after thermal annealing.

A single optical pulse with 50 ns width ($I = 560$ mA) was applied to the device attributing to a more amorphous state (weight '6', arbitrarily defined number) with an increase of $\sim 14\%$ in transmission, shown in Fig. 3a. At the same power setting, we applied a pulse train containing 100 pulses (50 ns width, 1 MHz repetition rate) to the photonic device which caused an abnormal decrease of the transmission with a lower weight achieved ('5'). Afterward, pulse trains containing 150, 200, 300, 500 and 1000 pulses were used to switch the device with lower transmission achieved in sequence (black arrow in Fig. 3a) corresponding to the weights 4, 3, 2, 1 and 0. Subsequently, we changed the weighting direction with number of pulses applied in a descending sequence (from 500 to 1) and the corresponding weights were achieved in the reverse order (weights 1 to 6). In other words, the weight of the photonic synapse, only determined by the number of the pulses (N), could be accessed by that number of pulse train from either weighting or switching directions.

The plasticity discussed above is demonstrated clearly by the plot of the optical transmission dependence on the pulse number, shown in Fig. 3b. Statistically, there is no difference of the optical transmission Fig. 2b. In addition, the transmission is exponentially decaying with increasing of the pulse number, which is fitted by the exponential function below:

$$T = T_0 + A \times e^{r \times N} \quad (2)$$

where, T_0 is the baseline of the transmission, while A and r are the fitting constants, as shown in Table 1.

Based on Hebbian leaning rule¹⁸, the synaptic plasticity in a biological system has the form of $\Delta w = A e^{-\Delta t/\tau}$, which is also known as the spike timing dependent plasticity (STDP). Here, Δw and Δt are the synaptic weight change and the time delay between pre- and post-neuron signals, while A and τ are constants. The fitting function (2) is very similar to the STDP form except the pulse number (N) rather than the time delay (Δt) dependent. We proposed an all-optical structure based on an interferometer to correlate Δt with N , using both the pre- and post-neuron signals to modulate the weight of the photonic synapse to mimic the STDP behavior.

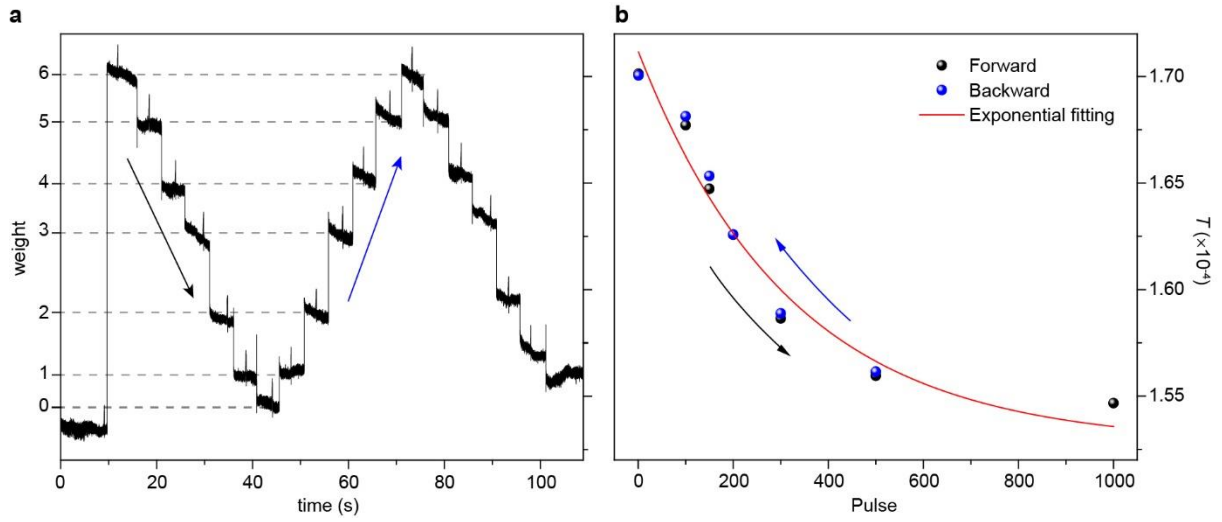


Figure 3. (a) Synaptic weighting of a photonic phase-change synapse using multiple optical pulses train. (b) Optical transmission (synaptic weight) as a function of the number of the optical pulses. Black and red sphere corresponds to forward (black arrow) and backward (red arrow) weighting direction respectively, as shown in (a). The red curve is the exponential fitting of the data.

Table 1. Parameters for the fitting used in Figs 2 and 3

Fitting function and parameters $T = T_1 + \frac{T_0 - T_1}{1 + (I/I_0)^p}$	Fig. 2			
	Forward (black)		Backward (red)	
	Mean	std	Mean	std
T_0	0.614×10^{-4}	0.871×10^{-6}	0.591×10^{-4}	0.259×10^{-6}
T_1	1.003×10^{-4}	1.342×10^{-6}	1.011×10^{-4}	0.434×10^{-6}
I_0	539.533	0.332	536.959	0.124
p	118.911	10.640	94.502	2.319
Adj. R-Square	0.9974		0.9997	
Fitting function and parameters $T = T_0 + A \times e^{r \times N}$	Fig. 3			
	Mean		std	
T_0	1.528×10^{-4}		1.472×10^{-6}	
A	1.844×10^{-5}		1.449×10^{-6}	
r	-0.312×10^{-2}		5.618×10^{-4}	
Adj. R-Square	0.9530			

4. CONCLUSIONS

In conclusion, we have demonstrated an integrated full-optical, non-volatile memory with multi-level (22 herein) storage in a single phase-change unit. By incorporating low dimensional phase-change materials (GST) on top of integrated silicon nitride waveguide, each level is stored as crystalline (amorphous) level in the GST and could be accessed directly by single optical pulse. The memory level has a Hill function dependent on the optical pulse power. The phase-change memory is promising to overcome the von Neumann bottleneck. In the meantime, we developed an all-optical photonic synapse by integrating multi GST units with tapered silicon nitride waveguide. The photonic synapse has a complete plasticity with synaptic weight exponentially dependent on the number of optical pulses applied. Utilizing an interferometer with full optical means, it's possible to reach STDP plasticity of the photonic synapse to mimic the neural synapse in functions. This development is a significant step for photonic neuromorphic computing.

ACKNOWLEDGEMENTS

The authors acknowledge support via the EPSRC Manufacturing Fellowship EP/J018694/1, the WAFT collaboration (EP/M015173/1) and the Champ Partnership (EP/M015130/1).

REFERENCES

- [1] Backus, J., "Can programming be liberated from von Neumann style?: a functional style and its algebra of programs," *Commun Acn* 21(8), 613-641 (1978).
- [2] Esser, S. K. et al., "Convolutional networks for fast, energy-efficient neuromorphic computing," *P Natl Acad Sci USA* 113(41), 11441-11446 (2016).
- [3] Hoang, B. and Hawkins, S. K., "How will rebooting computing help IoT?," 18th International Conference on Intelligence in Next Generation Networks, 121-127 (2015).
- [4] Indiveri, G., Chicca, E. and Douglas, R. J., "Artificial cognitive systems: from VLSI networks of spiking neurons to neuromorphic cognition," *Cogn Comput* 1(2), 119-127 (2009).
- [5] Caulfield, H. J. and Dolev, S., "Why future supercomputing requires optics," *Nat Photonics* 4(5), 261-263 (2010).
- [6] Kuramochi, E. et al., "Large-scale integration of wavelength-addressable all-optical memories on a photonic crystal chip," *Nat Photonics* 8(6), 474-481 (2014).
- [7] Reed, G. T., [Silicon photonics: the state of the art], John Wiley and Sons, Ltd, Chichester, UK (2008).
- [8] Rios, C. et al., "Integrated all-photonic non-volatile multi-level memory," *Nat Photonics* 9(11), 725-732 (2015).
- [9] Kandel, E. R., Schultz, J. H., Jessell, T. M., Siegelbaum, S. A. and Hudspeth, A. J., [Principles of neural science], McGraw-Hill, New York, fifth edition (2013).
- [10] Indiveri, G., Linares-Barranco, B., Legenstein, R., Deligeorgis, G. and Prodromakis, T., "Integration of nanoscale memoristor synapses in neuromorphic computing architectures," *Nanotechnology* 24(38), 384010 (2013)
- [11] Wuttig, M. and Yamada, N., "Phase-change materials for rewriteable data storage," *Nat Mater* 6(11), 824-832 (2007).
- [12] Yamada, N. and Matsunaga, T., "Structure of laser-crystallized $\text{Ge}_2\text{Sb}_{2+x}\text{Te}_5$ sputtered thin films for use in optical memory," *J Appl Phys* 88(12), 7020-7028 (2000).
- [13] Lankhorst, M. H. R., Ketelasrs, B. W. S. M. M. and Wolters, R. A. M., "Low-cost and nanoscale non-volatile memory concept for future silicon chips," *Nat Mater* 4(4), 347-352 (2005).
- [14] Wright, C. D., Hosseini, P. and Diosdado, J. A. V., "Beyond von-Neumann computing with nanoscale phase-change memory devices," *Adv Funct Mater* 23(18), 2248-2254 (2013).
- [15] Raoux, S., Xiong, F., Wuttig, M. and Prop, E., "Phase change materials and phase change memory," *Mrs Bull* 39(8), 703-710 (2014).
- [16] Ovshinsky, S. R., "Reversible electrical switching phenomena in disordered structures," *Phys Rev Lett* 21(20), 1450-1453 (1968).
- [17] Rios, C. Hosseini, P., Wright, C. D., Bhaskaran, H. and Pernice, W. H. P., "On-chip photonic memory elements employing phase-change materials," *Adv Mater* 26(9), 1372-1377 (2014).
- [18] Song, S., Miller, K. D. and Abbott, L. F., "Competitive Hebbian learning through spike-timing-dependent synaptic plasticity," *Nat Neurosci* 3(9), 919-926 (2000).